SWEPT SINE HUMIDITY SCHEDULE FOR TESTING CYCLE PERIOD EFFECTS ON CREEP[1]

Thomas J. Urbanik
Research Engineer

and

Sung K. Lee
Engineer

USDA Forest Service
Forest Products Laboratory
One Gifford Pinchot Drive
Madison, WI 53705-2398

(Received September 1993)

ABSTRACT

The stacking life of corrugated containers under load decreases as relative humidity (RH) increases and when RH cycles, compared with when RH remains stable. Conventional RH test schedules that rely on fixed cycle periods do not adequately reflect the significance of moisture diffusion and hygroexpansion rate phenomena on the creep of corrugated containers and general wood fiber products. With cycle periods shorter than a critical period, materials are relatively unaffected by cyclic changes in RH. Longer periods amplify material hygroexpansion and accelerate creep. In this study, we propose a swept sine RH schedule in which the cycle frequency varies logarithmically with time and set forth equations for generating a numerical control signal. Data from creep tests of corrugated fiberboard reveal the frequency dependence of the amplitude and phase relationships between cyclic hygroexpansion and cyclic RH. A swept sine RH schedule yielded the continuous form of the response characteristics varying with cycle period that could not be acquired with multiple constant period schedules. The critical cycle period and the hygroexpansion response to moisture as a function of cycle period are proposed as criteria for discriminating among hygroexpansion-creep models.

Keywords: Corrugated fiberboard, stacking life compression strength, cyclic humidity, testing.

INTRODUCTION

In the shipping and distribution system, corrugated fiberboard boxes are stacked and subjected to the weight of interior products and to unstable relative humidity (RH) levels. As the RH increases, paperboard moisture content increases and box strength decreases. Normal fluctuations in RH cause cyclical changes in paperboard moisture content and add to the severity of the strength decrease.

Containers experience humidity cycles caused by ambient weather fronts, diurnal changes, air handling equipment, and movement of containers between the warehouse and truck or rail car. These RH cycles occur with various frequencies. The cyclic RH will obviously change with the nature of the product and the distribution cycle. Yet the traditional methods of cyclic RH tests do not adequately address how to relate the stacking life of corrugated fiberboard to the environment.

In tests on paper subjected to tension creep (Gunderson and Tobey 1990) with RH cycling between 30% and 90% at various rates between a 20-min and a 168-h cycle period, the amount of creep per cycle remained constant. Rapid

[1] The Forest Products Laboratory is maintained in cooperation with the University of Wisconsin. This article was written and prepared by U.S. Government employees on official time, and it is therefore in the public domain and not subject to copyright.

Wood and Fiber Science, 27(1), 1995, pp. 68–78

cycling, i.e., short cycle periods, caused earlier specimen failures because more creep events occurred per interval of time.

However, in tests on corrugated boxes subjected to compression creep (Leake and Wojcik 1992), long RH cycle periods were more severe. Boxes survived for 15, 5, and 3 days when subjected to 50% to 90% RH cycles with 12-, 24-, and 48-h cycle periods, respectively. Boxes subjected to a constant 90% RH survived for 55 days. Because the constant RH environment is effectively a cyclic environment with an infinite cycle period, there should be a range of increasing periods beyond 48 h where stacking life first reaches a minimum and then increases.

More specific compression creep tests on a variety of corrugated fiberboard materials (Byrd and Koning 1978) corroborate the Leake and Wojcik (1992) box tests. In Byrd and Koning (1978), the creep rates of A-flute short column specimens subjected to 35% to 90% RH cycles were 3 to 14 times higher than similarly loaded specimens at a constant 90% RH. The higher the proportion of high-yield pulp, bark, or recycled content in a material, the higher the creep rate was for material subjected to cyclic RH; but these factors had little effect on materials at a constant RH. As with boxes, 24-h RH cycles were more severe than 3-h cycles in the short column tests. More specifically, the cycle period had more effect on creep rate for high-yield materials than for virgin commercial yield materials. Thus the expected performance of a material, compared to an average, depends on the RH cycle period.

In comparisons between the creep of the short columns and that of the short column components (Byrd 1984), the corrugated short columns crept 2 to 5 times faster than indicated by measurements of the components. Diffusion was believed to play a critical role in high-yield linerboards responding to moisture sorption more rapidly than conventional-yield linerboards and yielding higher creep rates.

A mechanosorptive model proposed for wood (Fridley et al. 1992) seems to reconcile the disparity between the paper tests and box tests. The creep rate of structural lumber in bending was assumed to be proportional to the rate of change of an average moisture content. Thus, beyond a critical RH cycle period long enough for moisture to diffuse to an equilibrium level, each moisture cycle would theoretically cause an equal amount of creep, as with paper. Because of the mass of cellulose fiber involved, the critical period for corrugated fiberboard and wood is probably long compared to that of paper. So the rate of average moisture content change, and therefore the creep rate, theoretically decreases as the RH cycle period decreases. Unfortunately, tests at only 24- and 96-h RH cycle periods (Fridley et al. 1990) were insufficient to quantify the model fully.

A practical upper limit on the RH cycle period for bending tests on particleboard (Gressel 1986) under a specific set of RH levels, specimen size, and load was shown to be around 96 h (McNatt 1993). The total creep, until 21 days, was found to increase as the RH cycle period increased but only up to a point. Beyond an RH cycle period of about 96 h, the 21-day creep remained about constant. Thus with long cycle periods, the creep per cycle was proportional to the cycle period. A significant number of tests with constant RH cycle periods would be required to generalize the conclusions to other specimen, load, and environmental conditions.

OBJECTIVE AND SCOPE

The objective of this study was to propose an experimental RH schedule that can be used to differentiate rapidly among the effects of various RH cycle periods on fiber product creep. A swept sine schedule for quantifying the significance of moisture diffusion on the hygroexpansion and creep response of corrugated fiberboard is introduced. The relevant equations for generating a numerical control signal and characterizing the resulting data are set forth.

Data on the performance of a USDA Forest Service, Forest Products Laboratory (FPL), test

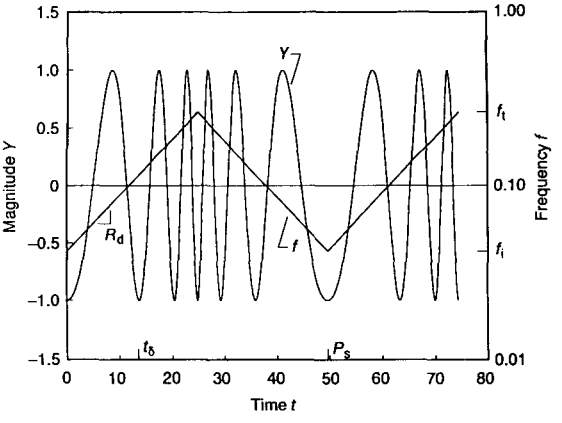

FIG. 1. Swept sine wave with $p_i = 24$, target $p_t = 4$, target $P_s = 48$, and $\phi = -\pi/2$ in which frequency varies logarithmically with time so that frequency change per cycle remains constant.

chamber controlled by a computer (Laufenberg 1991) showed that the RH level can be made to follow the form of a swept sine signal down to cycle periods as short as 1 h. Some specific creep tests of corrugated fiberboard, made by subjecting test specimens to the combined effects of a static weight and exposure to the cyclic RH, yielded the continuous form of the hygroexpansion amplitude and phase response varying with RH cycle period. Data were superior to those obtainable with multiple constant period schedules.

The scope of this work was limited to a demonstration of the compressive creep data that result from a swept sine humidity input. The form of the hygroexpansion-creep response as output to RH cycle period as input is proposed as criteria for the development of a model of the response and a determination of system characteristics from the data. The results of this report can have applications toward test methods for characterizing the hygroexpansion response of corrugated containers and relating creep to hygroexpansion.

SWEPT SINE THEORY

Basic equations

In Fig. 1, the form of a sine wave is shown in which frequency ω varies with time t, i.e., a swept sine wave. (In this report, when ω is used for frequency, units are radians per unit time. When f is used, units are cycles per unit time.) The case where ω varies logarithmically with t is of particular interest. In this case, the number of cycles during any time interval bounded by two frequencies with a fixed difference remains constant and independent of frequency. Therefore, a logarithmic sweep is a wise choice for testing the effect of cycle frequency on fatigue-sensitive materials.

To characterize the swept sine shape, the initial half-sweep during which ω sweeps from an initial frequency ω_i to a terminal frequency ω_t was first considered. For a logarithmic sweep, the sweep rate R_d is the rate of frequency change, in decades, per interval of time. Frequency varies according to

$$\omega(t) = \omega_i 10^{tR_d} \tag{1}$$

If a swept sine wave cycles with a constant amplitude B superimposed on a steady-state magnitude B_0, its cyclic magnitude Y at t depends on ω according to Eq. (1). The history of Y preceding t also needs to be accounted for. A formula that makes Y a function of ω and the Y-history during the first half-sweep is given by

$$Y(t) = B_0 + B \sin\left(\int_0^t \omega \, dt + \phi\right) \tag{2}$$

where ϕ is a phase angle characterizing the initial phase offset when $t = 0$. Substituting Eq. (1) into Eq. (2) and performing the integration yield

$$Y(t) = B_0 + B \sin \upsilon \tag{3}$$

where

$$\upsilon = \frac{\omega_i}{R_d \ln 10}(10^{tR_d} - 1) + \phi \tag{4}$$

After the first half-sweep, the sweep of the sine wave in Fig. 1 continues, and ω alternates between ω_i to ω_t and ω_t to ω_i. A single sweep period can be considered the sum of a first half-sweep at rate R_d and a second half-sweep of equal duration at rate minus R_d. The duration

of the sweep is the sweep period P_s, not to be confused with the sine wave period p where

$$p = \frac{2\pi}{\omega} \tag{5}$$

in which ω is given by Eq. (1). If a half-sweep over the time interval 0 to $P_s/2$ sweeps from frequency ω_i to ω_t, then the next half-sweep occurs over the interval $P_s/2$ to P_s of an equal duration, but sweeps from ω_t to ω_i. The sweep rate determined by using Eq. (1) and knowing that $\omega = \omega_t$ at $t = P_s/2$ is

$$R_d = \frac{\log(\omega_t/\omega_i)}{P_s/2} \tag{6}$$

Repeating sweeps

To characterize the shape of a swept sine wave in which ω repeatedly sweeps up and down, the integer values I_1 and J defined by the following equations are first needed:

$$I_1 = \text{Int}\left(\frac{2t}{P_s}\right) \tag{7}$$

and

$$J = \cos(I_1\pi) \tag{8}$$

In Eqs. (7) and (8), the Int function yields the integer component of its argument, and J therefore switches values between +1 and −1 for each half-sweep. Then values of $\hat{t}$, $\hat{R}_d$, $\hat{\omega}_i$, $\hat{\omega}_t$, $\hat{v}$, and $\hat{\phi}$ corresponding to t, R_d, ω_i, ω_t, v, and ϕ, respectively, can be determined and used in a way that accounts for each reversal of sweep direction. During each half-sweep $I_1 - 1$, the half-sweep time $\hat{t}$ varies from 0 to $P_s/2$ and is given by

$$\hat{t} = t - I_1 P_s/2 \tag{9}$$

The half-sweep rate $\hat{R}_d$, half-sweep initial frequency $\hat{\omega}_i$, and half-sweep terminal frequency $\hat{\omega}_t$ become the following, respectively:

$$\hat{R}_d = JR_d \tag{10}$$

$$\hat{\omega}_i = \frac{1+J}{2}\omega_i + \frac{1-J}{2}\omega_t \tag{11}$$

and

$$\hat{\omega}_t = \frac{1-J}{2}\omega_i + \frac{1+J}{2}\omega_t \tag{12}$$

Then frequency and magnitude can be characterized to deal with sweep direction according to

$$\omega(t) = \hat{\omega}_i 10^{\hat{t}\hat{R}_d} \tag{13}$$

and

$$Y(t) = B_0 + B \sin \hat{v} \tag{14}$$

respectively, where

$$\hat{v} = \frac{\hat{\omega}_i}{\hat{R}_d \ln 10}(10^{\hat{t}\hat{R}_d} - 1) + \hat{\phi} \tag{15}$$

The phase shift

$$\hat{\phi} = \phi + \frac{I_1\omega_i}{R_d \ln 10}(10^{P_s R_d/2} - 1) \tag{16}$$

accounts for the fact that for each half-sweep after the first half-sweep, the value of ϕ needs to be updated so that the magnitude of Y and rate of change dY/dt remain unchanged when the sweep reverses direction. The solution for $\hat{\phi}$ is obtained from Eq. (3) by equating Y at the termination of a half-sweep to Y at the initiation of the next half-sweep.

EXPERIMENTS

Tests were conducted in which corrugated fiberboard tubes, i.e., boxes without top and bottom flaps, were loaded under static compression and exposed to swept sine RH schedules. Tubes were fabricated from commercially purchased material of two flute constructions. The performance of a light grade single-walled material of nominal 1.21-MPa (175-lbf/in.^{2}) C-flute construction was compared with the performance of a heavy grade double-walled material of nominal 1.90-MPa (275-lbf/in.^{2}) CB-flute construction. The tubes were cut to form 305-mm (12-in.) cubes. Compression tests performed at 23 C (73 F) and 50% RH (ASTM 1990) yielded average strength values of 4.42 kN (994 lbf) and 9.54 kN (2,140 lbf) for the C-flute and CB-flute tubes, respec-

TABLE 1. *Swept sine schedules.*

Relative humidity schedule	p_i (h)	p_t (h)		P_s (h)		R_d (decades/h)	RH (%)	
		Target	Exact	Target	Exact		Minimum	Maximum
1	12	1	1.10	24	23.1	0.0899	53	89
2	24	0.5	0.506	48	47.8	0.0701	50	77
3	1	24	34.6	144	161	−0.0192	47	84
4	24	1	0.987	144	145	0.0192	49	84
5	4	400	757	2,000	2,277	−0.00200	46	83
6	24	4	3.77	48	49.6	0.0324	50	79

tively. The specimens were filled with soy beans, contained in a plastic bag, to about three-fourths of their volume; the intention was to cause the specimens to bulge outward, as filled boxes in service normally bulge.

A variety of swept sine RH schedules were tested to determine which schedule worked best. The parameters defining six schedules are given in Table 1. Note that p_t and P_s are specified in terms of target values and exact values. As explained in the Appendix, exact specifications determined from target specifications can be chosen to create repeating and symmetric half-sweeps. Although not critical for analyzing RH data, symmetric half-sweeps simplify the analysis of deformation data. For all tests, the temperature was maintained at 23 C (73 F).

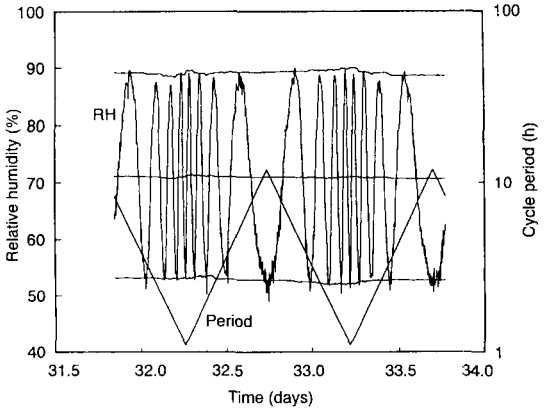

FIG. 2. Variation of relative humidity with time following swept sine control signal. Lines through approximate steady-state, maximum, and minimum values represent moving window, three-cycle band width fit to data of swept sine wave defined by $p_i = 12$, target $p_t = 1$, target $P_s = 24$, and $\phi = -\pi/2$.

Relative humidity excitation

In humidity schedule 1 (Fig. 2), the RH level H was made to follow a numerical control signal according to Eq. (14). An RH sensor was placed within the circulation exhaust duct of the test chamber, and moisture was added to or subtracted from the air intake to make the sensor follow the control signal. Parameters B_0 and B characterizing the control signal are exact. However, in practice, errors between H and the programmed RH level result from mechanical fluctuations and unpredictable adsorption and desorption phenomena of hygroscopic material within the chamber. Therefore, the respective averages $\bar{B}_0$ and $\bar{B}$ are introduced to characterize the variation of H with time according to

$$H(t) = \bar{B}_0 + \bar{B} \sin \hat{v} \qquad (17)$$

in which $\hat{v}$ is given by Eq. (15). Given the variation of H with sin $\hat{v}$ data from the data window bounded by

$$t_1 \leq t < t_2 \qquad (18)$$

a determination of $\bar{B}_0$ and $\bar{B}$ according to Eq. (17) yields an average characterization of the RH around t. The performance of the long-term RH schedule was more specifically quantified by performing a moving window analysis in which the t_1–t_2 window was moved along the curve of H varying with t, and plots of the steady-state $\bar{B}_0$, maximum $\bar{B}_0 + \bar{B}$, and minimum $\bar{B}_0 - \bar{B}$ values varying with t were superimposed (Fig. 2). The number of RH cycles N_2 per data window was fixed at 3.

Relative humidity schedule 2 (Fig. 3) was used to determine how rapidly the FPL test

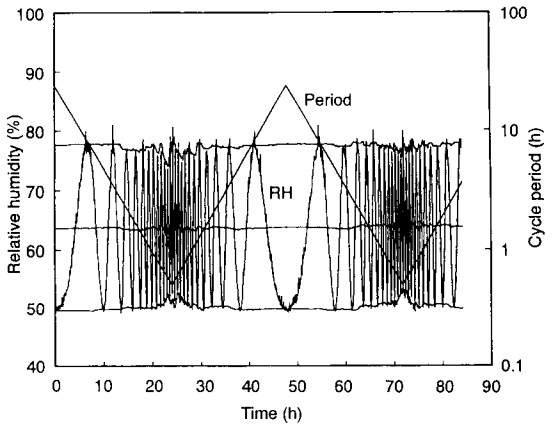

FIG. 3. Variation of relative humidity with time following swept sine control signal. The lines through approximate steady-state, maximum, and minimum values represent moving window, one-cycle band width fit to data of swept sine wave defined by $p_i = 24$, target $p_t = 0.5$, target $P_s = 48$, and $\phi = -\pi/2$.

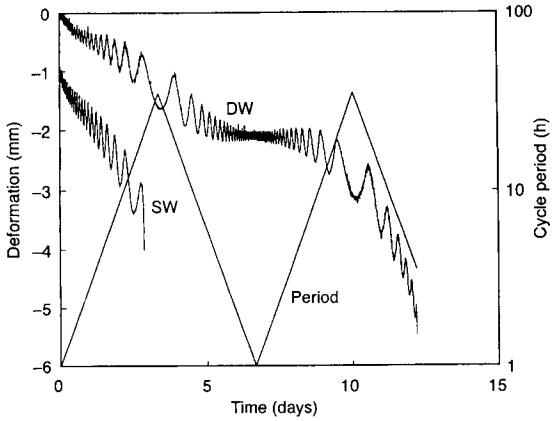

FIG. 4. Variation of deformation of single-walled (SW) and double-walled (DW) corrugated fiberboard tubes with time, when subjected to static load equal to 25% of tube compression strength and swept sine relative humidity excitation.

chamber could respond to RH changes. A moving window analysis performed with $N_2 = 1$ yielded a more critical test of the RH characterization at short cycle periods than did the analysis of Fig. 2. According to the results in Fig. 3, the FPL test chamber can generate RH cycle periods as short as 1 h. Additional tests are needed to examine if the hygroexpansion response of test specimens varies with position within the chamber. Our moving window procedure is a good tool for performing these tests.

Deformation response

Typical plots of specimen deformation compared with time, corresponding to RH schedules 3 to 5 (Table 1) are shown in Figs. 4 to 6. The deformations, plotted with respect to an arbitrary zero-level reference, are the sum of hygroexpansion caused by moisture content and creep caused by stress. The hygroexpansion amplitude shows an obvious dependence on the cycle frequency, particularly in Fig. 5. High frequencies do not allow sufficient time for moisture to diffuse and build up in the material.

The effect of cycle frequency on the creep rate is most apparent in Fig. 4, which corresponds to RH schedule 3. A similar effect can be seen in Fig. 5 (RH schedule 4) but to a lesser degree. The creep rate increases as the cycle frequency decreases. In Fig. 4, creep seems to stop when RH cycles at high frequencies.

The data in Fig. 4 are from a cyclic creep test initiating at a short cycle period, i.e., 1 h. Test specimens were loaded to 25% of their respective compression strengths. The load level was too severe because a secondary creep

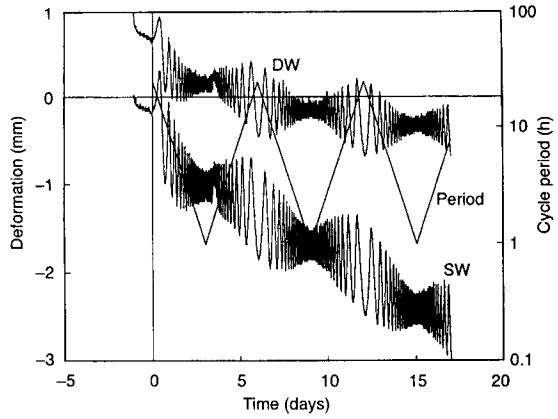

FIG. 5. Variation of deformation of single-walled (SW) and double-walled (DW) corrugated fiberboard tubes with time, when subjected to static load equal to 17% of tube compression strength and swept sine relative humidity excitation.

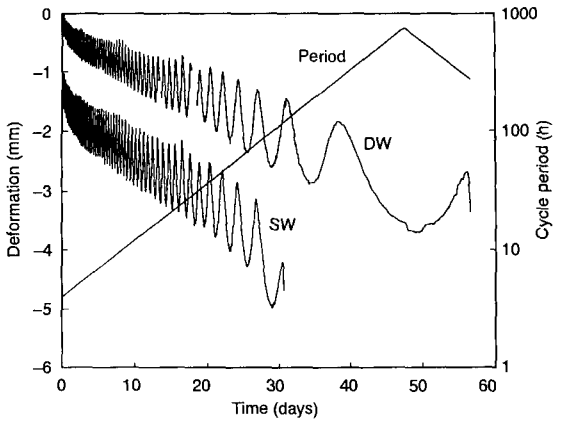

FIG. 6. Variation of deformation of single-walled (SW) and double-walled (DW) corrugated fiberboard tubes with time, when subjected to static loads equal to 13% and 17%, respectively, of tube compression strength and slow sweep rate, and swept sine relative humidity excitation.

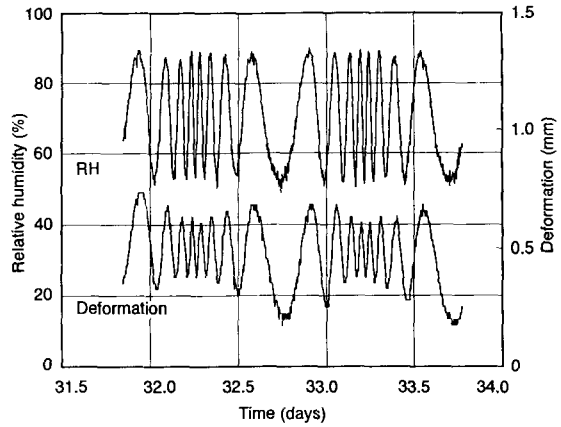

FIG. 8. Upper curve: Relative humidity compared with time from Fig. 2. Lower curve: Variation of deformation of corrugated fiberboard tube with time when subjected to humidity excitation.

response following a primary or "break-in" response was not discernible from the data. Thus, load levels of about 17% and RH schedule 4, beginning with a 24-h period, were tested next (Fig. 5). Furthermore, the cyclic creep test was preceded by a short, constant RH test to condition the specimens. A secondary creep response with repetitive sweeps is more apparent in the data.

Figure 6, in which RH schedule 5 was used, is the result of a swept sine creep test at a very low sweep rate. A long cycle period, beyond which the creep rate would decrease, was sought. The single-walled specimen was loaded to 13% of its strength, and the double-walled specimen was loaded to 17% of its strength. Testing began at high-cycle frequencies to obtain a secondary creep response during the low frequencies of interest. The secondary creep rate seems to remain constant, and the hygroexpansion amplitude seems to increase continuously with an increasing RH cycle period, even through the final 14-day half-sweep cycle period. In Fig. 7, the same deformation data are plotted with the RH cycle frequency. Using a logarithmic sweep yielded equal-width cycles. Thus there are an equal number of cycles between frequencies 1 and 2 cycles per day and between frequencies 4 and 5 cycles per day; and fatigue effects were made independent of frequency. A rapid increase in the creep per RH cycle was apparent when the cycle period exceeded 1 day.

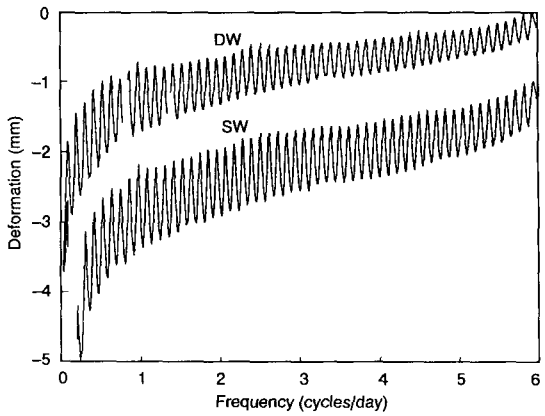

FIG. 7. Deformation data from Fig. 6 compared with RH cycle frequency.

Figure 8 shows more closely how the hygroexpansion response followed the RH excitation. The peaks in the response curve, e.g., at t = 32.5 and t = 33 days, lagged behind the input. The amplitude and phase relationships in Fig. 8 become more recognizable if data are plotted in the form of a Lissajous diagram (Beckwith and Buck 1969) (Fig. 9). About 6 h of data were used for the relationships in Fig.

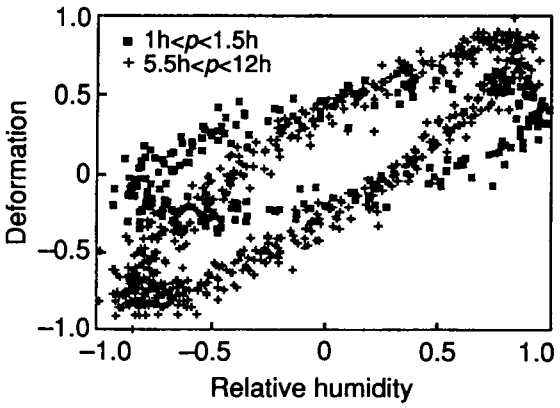

FIG. 9. Lissajous diagram of data with form shown in Fig. 8. Scales are normalized with respect to ±1.

9, and the creep component of deformation was subtracted, assuming a linear creep rate. Data were divided into low-frequency and high-frequency subsets. In the elliptical patterns shown, the top of the ellipse corresponds to an increasing RH and the bottom of the ellipse corresponds to a decreasing RH.

Horizontal tangents to the minimum and maximum of an ellipse establish the amplitude of the hygroexpansion response. From the data in Fig. 9, the y-axis amplitude levels attained were about 0.6 and 0.3, following adsorption and desorption, respectively, when 1 h $\leq$ p $\leq$ 1.5 h and about 0.8 and 0.8 when 5.5 h $\leq$ p $\leq$ 12 h. Thus, the hygroexpansion amplitude response to cyclic RH was less symmetrical at high cycle frequencies. The intersection of the ellipse with the y-axis was used to determine the phase lag θ of the response with respect to input, using the relationship

$$\sin \theta = \frac{\text{y-intercept}}{\text{y-amplitude}} \tag{19}$$

From Fig. 9, the respective adsorption and desorption intercept levels were 0.4 and 0.25 when 1 h $\leq$ p $\leq$ 1.5 h and 0.4 and 0.3 when 5.5 h $\leq$ p $\leq$ 12 h to yield θ values of 42°, 56°, 30°, and 22°, respectively. Thus, at high RH cycle frequencies, the desorption hygroexpansion response was more out of phase with the forcing RH compared to the adsorption hygroexpansion; at low RH cycle frequencies, the reverse was found.

Our data (Figs. 4–7, 9) reveal that hygroexpansion amplitude A and phase lag θ relative to RH vary with RH cycle frequency. The constant frequency creep model (Urbanik 1994) can be applied to a short time interval of the data if the frequency change during the interval is small and the frequency dependence of amplitude and phase lag can be neglected. Specimen deformation in Urbanik (1994) was the sum of hygroexpansion caused by moisture content and mechanosorptive creep caused by

TABLE 2. *Deformation response characterization for short* $t_1 \leq t \leq t_2$.

Name	Expression
Hygroexpansion function	$x_h(t) = A_0 + A \sin \hat{\mu}$
Steady-state magnitude	A_0
Hygroexpansion amplitude	A
Phase lag relationship	$\hat{u} = \hat{v} - \theta - \theta_0 \cos(\hat{v} - \theta)$
Average phase lag	θ
Phase lag addition/subtraction	θ_0
Hygroexpansion rate	$dx_h/dt = A\omega(t)\hat{\beta} \cos \hat{u}$
Phase angle term	$\hat{\beta} = \theta_0 \sin(\hat{v} - \theta) + 1$
Instantaneous creep rate	$dx_c/dt = \mu \lvert dx_h/dt \rvert = A\mu\omega(t) \lvert \hat{\beta} \cos \hat{u} \rvert$
Mechanosorptive creep constant	μ
Mechanosorptive creep function	$x_c(t) = A\mu \int_{t_1}^{t_2} \omega(t) \lvert \hat{\beta} \cos \hat{\mu} \rvert dt$
Function evaluation	$x_c(t) = A\mu[C_i(t)]_{t_1}^{t_2} + X_0$
Interval initial creep	$X_0 = x_c(t_1)$
Integral evaluation	$C_i(t) = \sin \hat{u}$ sign $(\hat{\beta} \cos \hat{u}) + 2I_4$
Half-sweep counter	$I_4 = (\hat{v} - \tan^{-1}(\tan \hat{u}))/\pi$
Deformation function	$X(t) = x_h(t) + x_c(t)$

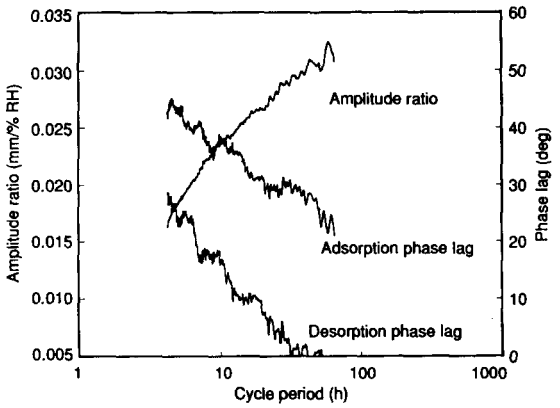

FIG. 10. Variation with cycle period of amplitude and phase response characteristics of single-walled corrugated fiberboard subjected to stress and cyclic relative humidity (RH). The amplitude ratio is between the hygroexpansion amplitude and RH amplitude. The phase lags are maximum and minimum values attained during adsorption and desorption, respectively.

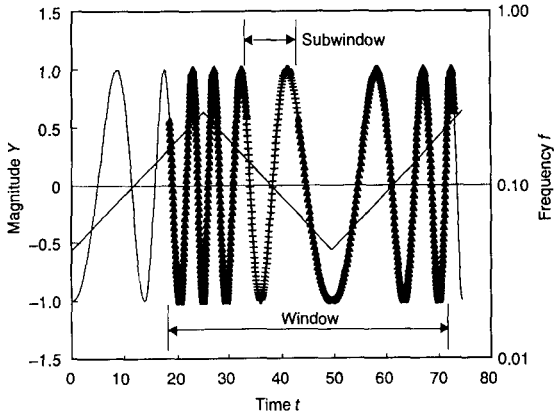

FIG. 12. Swept sine wave with $N_1 = 3$ cycles per half-sweep, window with $N_2 = 7$ cycles between times $t_1 = 18.4$ and $t_2 = 73$, and subwindow with $N_3 = 1$ cycle between frequencies $f_1 = 0.14$ and $f_2 = 0.07$ at respective times $\tilde{t}_1 = 33$ and $\tilde{t}_2 = 43$.

the cumulative ratcheting of swelling and shrinking effects with each change in specimen moisture content. The instantaneous creep rate was proportional to the nondirectional rate of hygroexpansion.

The derivation of a deformation function X(t) in Urbanik (1994) is expanded in Table 2 for the case of a swept sine RH excitation

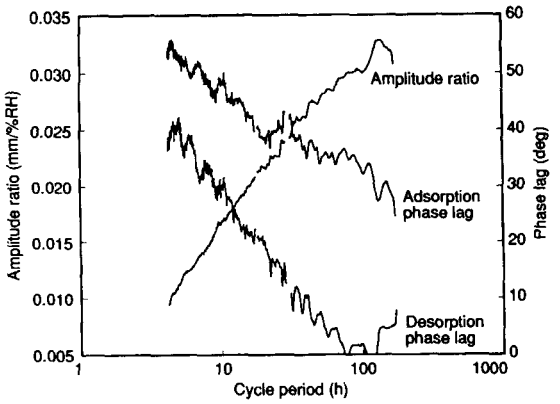

FIG. 11. Variation with cycle period of amplitude and phase response characteristics of double-walled corrugated fiberboard subjected to stress and cyclic relative humidity (RH). The amplitude ratio is between the hygroexpansion amplitude and RH amplitude. The phase lags are maximum and minimum values attained during adsorption and desorption, respectively.

during a short time interval t_1–t_2. A phase lag that varies empirically, up to a value $\pm\theta_0$, with the direction and rate of hygroexpansion, is introduced. The result is a model applicable to a short data window of the low R_d response (Fig. 6). An estimate of the hygroexpansion response variation with frequency is obtainable by fitting X(t) to a moving window of deformation data.

Figure 10 shows an analysis of the previous single-walled hygroexpansion data (Fig. 6). A 3-cycle moving window was used to determine values of the hygroexpansion amplitude, maximum phase lag $\theta + \theta_0$ during adsorption, and the minimum phase lag $\theta - \theta_0$ during desorption as they vary with RH cycle frequencies. The amplitude ratio $A/\bar{B}$ is plotted (Fig. 10) to smooth the effects of RH fluctuations. A steady-state condition, recognizable by an upper RH cycle period when the amplitude ratio and phase lag level off, was not reached in the test.

Figure 11 shows a similar analysis of the double-walled data (Fig. 6). A comparison of Figs. 10 and 11 reveals how moisture diffusion affects the hygroexpansion response times between single-walled and double-walled material, respectively. Data in the form of Figs. 10

and 11 are a critical test of proposed hygroexpansion models.

CONCLUSIONS

Conventional RH schedules for cyclic humidity tests do not adequately reveal the significance of moisture diffusion phenomena on the creep of corrugated containers and general wood fiber product. With a swept sine RH schedule in which frequency varies logarithmically with time, the effect of RH cycle period on hygroexpansion and creep performance becomes significantly more evident. The hygroexpansion amplitude and the creep rate increase as the cyclic RH period increases. Creep can terminate if the RH cycles faster than the ability of moisture to diffuse in and out of the material. Additional research is needed to relate the creep response to the hygroexpansion rate characteristics of a material. A moving window analysis procedure, given in this report for characterizing swept sine RH performance, can be extended to reduce deformation data and discriminate among potential hygroexpansion and creep models. Just as swept sine vibration tests are used to determine the relevant mechanical performance of a package system, the procedures of this report can more rapidly identify inferior moisture response characteristics of corrugated containers and characterize the severity of uncontrolled cyclic RH environments.

REFERENCES

ASTM. 1990. Standard test method for determining compression resistance of shipping containers, components, and unit loads. ASTM D642. American Society for Testing and Materials, Philadelphia, PA.

BECKWITH, T. G., AND N. L. BUCK. 1969. Mechanical measurements. Addison-Wesley Pub. Co. Inc., Reading, MA.

BYRD, V. L. 1984. Edgewise compression creep of fiberboard components in a cyclic-relative-humidity environment. Tappi 67(7):86–90.

BYRD, V. L., AND J. W. KONING, JR. 1978. Edgewise compression creep in cyclic relative humidity environments. Tappi 61(6):35–37.

FRIDLEY, H. J., R. C. TANG, AND L. A. SOLTIS. 1990. Moisture effects on load-duration behavior of lumber. Part II. Effect of cyclic relative humidity. Wood Fiber Sci. 24(1):89–98.

———, ———, AND ———. 1992. Creep behavior model for structural lumber. J. Struct. Eng. 118(8):2261–2277.

GRESSEL, V. P. 1986. A proposal for consistent experimental principles for conducting and evaluating creep tests. Holz Roh-Werkst. 44(4):133–138.

GUNDERSON, D. E., AND W. E. TOBEY. 1990. Tensile creep of paperboard—Effect of humidity change rates. Pages 213–226 *in* Proceedings, Materials Interactions Relevant to the Pulp, Paper, and Wood Industries. Materials Research Society, Pittsburgh, PA.

LAUFENBERG, T. L. 1991. Characterization of paperboard, combined board, and container performance in the service moisture environment. Pages 300–302 *in* Proceedings, TAPPI, International Paper Physics Conference, Kona, HI.

LEAKE, C., AND R. WOJCIK. 1992. Humidity cycling rates: How they affect container life spans. Pages 134–144 *in* Proceedings, Cyclic Humidity Effects on Paperboard Packaging. Forest Products Laboratory, Madison, WI.

MCNATT, J. D. 1993. Moisture—A critical element in duration-of-load/creep research. Proceedings, Oriented Structural Board: Duration of Load Performance. Structural Board Association Workshop, February 16–18. Toronto, Ontario, Canada.

URBANIK, T. J. 1994. Hygroexpansion-creep model for corrugated fiberboard. Proposed for Wood and Fiber Science.

APPENDIX

Creating symmetrical half-sweeps

The analysis of swept sine data is simplified if, given ω_i and R_d, ω_t and ϕ are chosen such that half-sweeps become symmetrical and repeat. To do this, note that the time duration t_δ of the first cycle in Fig. 1 is determinable from Eq. (3) using $Y(0) = Y(t_\delta)$.

$$t_\delta = \frac{\log(1 + 2\pi R_d \ln 10/\omega_i)}{R_d} \tag{20}$$

From Eq. (1), the corresponding frequency change ω_δ is

$$\omega_\delta = \omega(t_\delta) - \omega_i \tag{21}$$

With each cycle, the frequency changes by the same amount, i.e., ω_δ. Therefore, if a value for ω_t is chosen such that

$$\omega_t = \omega_i + N_1\omega_\delta \tag{22}$$

where N_1 is an integer, each half-sweep will consist of N_1 cycles and the sweeps will repeat. Additionally, if $\phi = \pm\pi/2$, each half-sweep will be a symmetrical image of the previous half-sweep.

In specifying the parameters of a swept sine wave for use as a controlled input to a test, it is convenient to work with the time characteristics p_i, p_t, and P_s where p_i and p_t correspond to ω_i and ω_t, respectively in terms of Eq. (5). An exact value of p_i and target values of p_t and P_s should

first be chosen. Then, given an integer value of N_1 determined from

$$N_1 \approx \frac{\omega_t - \omega_i}{\omega_\delta} \tag{23}$$

using Eqs. (6), (20), and (21). Equation (22) yields the exact ω_t value and thus p_t. Using Eq. (6), the exact value for P_s becomes

$$P_s = \frac{2\log(\omega_t/\omega_i)}{R_d} \tag{24}$$

In applications where the test response is expected to be sensitive to the sweep rate, the swept sine wave should be specified in terms of p_i, p_t, and R_d. An approximate value of p_t can first be chosen. Then exact values of p_t and P_s can be determined as previously discussed.

Constant band width algorithm

The moving window analysis yields a more accurate evaluation of the effect of cycle frequency on H performance if t_1 and t_2 are chosen such that the number of RH cycles N_2 within each data window remains constant. The strategy to do this for an arbitrarily wide window is to (1) look for a subwindow for which the time duration does not exceed P_s, (2) determine the end frequencies ω_1 and ω_2 of the subwindow and corresponding times $\bar{t}_1$ and $\bar{t}_2$, respectively, and (3) account for the time difference between the whole window and the subwindow.

The number of RH cycles N_3 within the appropriate subwindow is

$$N_3 = N_2 - 2N_1I_2 \tag{25}$$

where

$$I_2 = \text{Int}\left(\frac{N_2}{2N_1}\right) - \text{Int}\left(\frac{\text{Int}(N_2/2N_1)}{N_2/2N_1}\right) \tag{26}$$

Taking the ω value corresponding to t as the center frequency of the window, $\bar{t}_1$ and $\bar{t}_2$ are determinable once ω_1 and ω_2 are known. If the sweep direction remains continuous from either $\bar{t}_1$ to t or t to $\bar{t}_2$, the respective end frequency is simply $\omega \pm \omega_\gamma$ where

$$\omega_\gamma = \omega_\alpha \frac{N_3}{2N_1} \tag{27}$$

and

$$\omega_\alpha = |\omega_t - \omega_i| \tag{28}$$

Otherwise, the frequency change in a half-window must be separated into up-sweep and down-sweep components. Figure 10 shows the significance of the various values of N, t, and ω.

The direction of the frequency sweep and the change in direction between half sweeps must be accounted for throughout the data window. Therefore, the following algorithm is provided and yields a function W(T, Ω, m) for determining the correct $\bar{t}_m$ values from T = t and $\Omega = \omega_\gamma$ for m = 1, 2. In the algorithm, values of J, $\hat{t}$, $\hat{R}_d$, $\hat{\omega}_i$, $\hat{\omega}_t$, and ω are to be evaluated at T by Eqs. (8) to (13), respectively. Parameter K equals +1 or −1 corresponding to an increasing or decreasing frequency, respectively, around ω. The L takes on a value of +1 or −1 to yield a KL value that either equals +1 when the sweep direction within the respective half-window remains constant or switches to −1 when the sweep reverses direction.

From

$$K = \hat{R}_d/|R_d| \tag{29}$$

and

$$L_m = 2\text{Int}\{\tanh[(2 - m)(\omega - \hat{\omega}_i) + (m - 1)(\hat{\omega}_t - \omega) - K\Omega] + 1\} - 1 \qquad m = 1, 2 \tag{30}$$

the end frequencies of the subwindow are given by

$$\omega_m = KL_m\omega + (2m - 3)L_m\Omega + (1 - KL_m)[(2 - m)\hat{\omega}_i + (m - 1)\hat{\omega}_t] \qquad m = 1, 2 \tag{31}$$

The expression on the right in Eq. (31) reduces to $\omega \pm \omega_\gamma$ when KL = 1. Using the half-sweep time values $\hat{t}_1$ and $\hat{t}_2$ given by

$$\hat{t}_m = \frac{\log(\omega_m/\hat{\omega}_i)}{\hat{R}_d} \qquad m = 1, 2 \tag{32}$$

the subwindow end times are given by

$$\bar{t}_m = W(t, \omega_\gamma, m) \qquad m = 1, 2 \tag{33}$$

where

$$W(T, \Omega, m) = T - \hat{t} + KL_m\hat{t}_m + \frac{(m - 1)(1 - KL_m)P_s}{2} \qquad m = 1, 2 \tag{34}$$

in which Eqs. (29) to (32) are used.

With N_3 defined by Eq. (25), the time difference between the whole window and the subwindow becomes a multiple of P_s. Therefore, by using $\bar{t}_m$ and ω_α as input to W, the window end times of interest can be determined from

$$t_m = \bar{t}_m + \frac{1 - \cos(I_2\pi)}{2}[W(\bar{t}_m, \omega_\alpha, m) - \bar{t}_m] + (2m - 3)\text{Int}\left(\frac{I_2}{2}\right)P_s \qquad m = 1, 2 \tag{35}$$

For a small window, the moving window analysis proposed here simulates the performance of an electronic tracking filter and a fixed band width for reducing vibration data.